Mathematical Models of Cochlear Nucleus Onset Neurons: I. Point Neuron with Many Weak Synaptic Inputs

SRIDHAR KALLURI and
Speech and Hearing Sciences Program, Harvard University–Massachusetts Institute of Technology, Division of Health Sciences and Technology; Eaton-Peabody Laboratory, Massachusetts Eye and Ear Infirmary, 243 Charles St., Boston, MA 02114 sridhar kalluri@alum.mit.edu

BERTRAND DELGUTTE
Eaton-Peabody Laboratory, Massachusetts Eye and Ear Infirmary, 243 Charles St., Boston, MA 02114; Research Laboratory of Electronics, Massachusetts Institute of Technology; Speech and Hearing Sciences Program, Harvard University–Massachusetts Institute of Technology, Division of Health Sciences and Technology

Abstract

The cochlear nucleus (CN) presents a unique opportunity for quantitatively studying input-output transformations by neurons because it gives rise to a variety of different response types from a relatively homogeneous input source, the auditory nerve (AN). Particularly interesting among CN neurons are Onset (*On*) neurons, which have a prominent response to the onset of sustained sounds followed by little or no response in the steady-state. *On* neurons contrast sharply with their AN inputs, which respond vigorously throughout stimuli. *On* neurons can entrain to stimuli (firing once per cycle of a periodic stimulus) at up to 1000 Hz, unlike their AN inputs. To understand the mechanisms underlying these response patterns, we tested whether an integrate-to-threshold point-neuron model with a fixed refractory period can account for *On* discharge patterns for tones, systematically examining the effect of membrane time constant and the number and strength of the exclusively excitatory AN synaptic inputs. To produce both onset responses to high-frequency tone bursts and entrainment to a broad range of low-frequency tones, the model must have a short time constant (≈0.125 ms) and a large number (>100) of weak synaptic inputs, properties that are consistent with the electrical properties and anatomy of *On*-responding cells. With these parameters, the model acts like a coincidence detector with a threshold-like relationship between the instantaneous discharge rates of the output and the inputs. Onset responses to high-frequency tone bursts result because the threshold effect enhances the initial response of the AN inputs and suppresses their relatively lower sustained response. However, when the model entrains across a broad range of frequencies, it also produces short interspike intervals at the onset of high-frequency tone bursts, a response pattern not found in all types of *On* neurons. These results show a tradeoff, that may be a general property of many neurons, between following rapid stimulus fluctuations and responding without short interspike intervals at the onset of sustained stimuli.

Keywords

integrate-and-fire model; coincidence detection; cochlear nucleus

1. Introduction

The cochlear nucleus (CN) gives rise to parallel pathways along which information about acoustic stimuli is processed and transmitted to more central stations in the auditory system (Kiang et al., 1973; Cant, 1992). While auditory-nerve (AN) fibers, all of which synapse on neurons in the CN (de No, 1981; Liberman, 1991, 1993), respond to sound in broadly similar ways (Kiang et al., 1965), CN neurons exhibit a wide variety of response types. The different types of CN neurons project to different nuclei in the auditory brainstem and midbrain, so that the parallel pathways arising in the CN convey selective information about sound to their central targets (Kiang et al., 1973).

Onset (*On*) neurons, the subject of this study, are one of three major types of neurons in the ventral division of the CN (VCN) (Pfeiffer, 1966); the other main types are chopper and primary-like neurons. *On* neurons are named for their transient response to the onset of stimuli, with little or no response in the steady-state. These responses are in sharp contrast to the vigorous sustained responses of AN fibers and other VCN neurons.

On neurons are of interest to auditory scientists because onset transients in sound are important for speech perception (Stevens, 1995), music perception (Deutsch, 1982), sound localization (Zurek, 1987), as well as segregation and grouping of sound sources (Bregman, 1990). Several possible functions have been proposed for CN *On* neurons, including the precise coding of sound intensity (Rhode and Smith, 1986; Winter and Palmer, 1995), the coding of pitch and amplitude modulation (Kim et al., 1990; Frisina et al., 1990; Rhode and Greenbert, 1994; Shofner et al., 1996; Evans and Zhao, 1997), as well as general alerting functions. An important prerequisite for determining the function of *On* neurons is understanding how they respond to biologically significant sounds such as speech and music, a task that would be considerably eased by a mechanistic understanding of how *On* neurons produce their characteristic responses to sound. This quantification of input-output relations in CN *On* neurons is the goal of our study.

On discharge patterns are recorded from all three major cell types in the VCN: stellate, bushy, and octopus cells. These cell types differ in morphology (Rhode et al., 1983; Rouiller and Ryugo, 1984), electrical properties (Oertel, 1983; Wu and Oertel, 1984; Manis and Marx, 1991), and synaptic organization (Morest et al., 1973; Brawer et al., 1974, Liberman, 1991; Cant, 1992; Liberman, 1993). Correspondingly, there is a great deal of heterogeneity within the class of *On* neurons, which are commonly divided into three groups based on the shape of their response patterns for high-frequency tone bursts (Godfrey et al., 1975b; Rhode and Smith, 1986; Winter and Palmer, 1995) shown in Fig. 1: (1) ideal onset (*On-I*), (2) onset with late or long-lasting activity (*On-L*), and (3) onset with chopping (*On-C*). Because most synaptic inputs to these neurons are from the same, relatively homogeneous source, the AN, the variations in response properties of *On* neurons must arise from differences in the underlying cellular properties (Kiang et al., 1973; Morest et al., 1973). Thus, *On* neurons (and VCN neurons in general), present a unique opportunity for quantitatively testing hypotheses about how cellular properties shape input-output relations in neurons.

Despite the heterogeneity in response properties of *On* neurons, the different cells that give rise to *On* discharge patterns all have characteristics in common: a large number of small synapses (Kane, 1973; Smith and Rhode, 1989; Liberman, 1991, 1993), extremely short membrane time constants (Wu and Oertel, 1984; Oertel et al., 1990; Manis and Marx, 1991; Golding et al., 1995), and morphological characteristics of electrically small cells such as large, spherical cell bodies and thick, nontapering dendrites (Kane, 1973; Smith and Rhode, 1987, 1989; Cant and Morest, 1979; Tolbert and Morest, 1982; Oertel et al., 1990; Golding et al.,

1995). These common properties provide guidelines for developing a general model of *On* neurons that would be applicable to all subtypes with simple adjustments in model parameters.

This article is the first of two that use mathematical models to test hypotheses about cellular characteristics of *On* neurons. In this article, we systematically examine the effects of the membrane time constant and the number and strength of synapses on the ability of an integrate-to-threshold point-neuron model (known as the leaky-integrator model in the remainder of the paper) to predict two key response properties of *On* neurons: Onset peri-stimulus time (PST) histograms for high-frequency tone bursts and entrainment to low-frequency tones (i.e., ability to discharge once on every cycle of a periodic stimulus). We show that the leaky integrator model can produce these two response properties but only for *On-C* neurons. In the subsequent article, we introduce a modification to the membrane spike generator that allows the model to simulate response patterns and entrainment for all three groups of *On* neurons.

Neurons that produce both entrainment and *On* PST histograms are interesting because the combination is infrequently observed in sensory neurons and the responses contrast dramatically with those of AN fibers. Entrainment to tones up to 1000 Hz requires neurons to produce interspike intervals of 1 millisecond, near the lower limit set by the absolute refractory period of most neurons. On the other hand, to produce *On* PST histograms, a neuron must prevent short interspike intervals, signifying a high discharge rate, during the steady-state of high-frequency tone bursts.

Previous models of *On* neurons have pointed out that fast membrane dynamics and weakly-excitatory synapses requiring coincidence of many inputs suffice to produce *On* PST histograms for high-frequency tone bursts (Rothman et al., 1993; Rothman and Young, 1996; Kipke and Levy, 1997, 1998). On the other hand, other models have attributed key roles to inhibitory inputs (Eriksson and Robert, 1999) and special voltage-gated ion channels found in some *On* neurons (Arle and Kim, 1991; Cai et al., 1997; Evans, 1998; Cai et al., 2000). None of these previous efforts has examined in detail the model's ability to produce entrainment to a wide range of tone frequencies.

Preliminary reports of this work have been presented (Kalluri and Delgutte, 1996, 1997, 2001).

2. Methods

The model for *On* neurons is a cascade of two stages. The first stage is a model for the response of AN fibers to sound and the second stage is the model for a CN neuron whose output is the time of occurrence of spikes.

2.1. Model of Auditory-Nerve Fibers

Discharge patterns on AN fibers were simulated using a computational model (Carney, 1993) that includes the following features.

1. The band-pass tuning of AN fibers is modeled by a gamma-tone filter (Johannesma, 1972). In the original implementation of the Carney (1993) model, the level-dependent tuning of AN fibers was modeled by making the bandwidth of the gamma-tone filter vary with the instantaneous amplitude of the input. We modified this model by fixing the filter bandwidth during a stimulus according to the overall stimulus level, thus making our impllementation most suitable for modeling the discharge patterns for stationary stimuli. The time-invariant bandwidth was preferred to the original model of Carney (1993) because the time-varying filter introduced response

components at harmonics of low-frequency tones, which are not found in responses of real AN fibers.

2. The fall in phase-locking as a function of frequency is modeled by a second-order low-pass filter with a cutoff frequency of 1 KHz.

3. Adaptation of firing rate is described using a model of the inner hair cell synapse (Westerman and Smith, 1988). Briefly, the model synapse has a high-pass filtering effect on its input. The discharge rate peaks when the stimulus has a rapid amplitude increase, as at the onset, and it falls to a lower value when the stimulus amplitude settles to a steady state. The model accurately simulates the adaptation characteristics of high-spontaneous-rate AN fibers.

4. To describe the stochastic nature of spike discharges, the spike train on a single fiber is modeled as a nonstationary renewal process whose instantaneous probability of discharge is the product of a component representing excitatory drive from hair cells and a component representing refractory properties (Johnson and Swami, 1983). Spikes for each AN fiber are generated using independent random number generators.

2.2. The Leaky-Integrator Model

The leaky-integrator model used to describe synaptic integration and spike generation by *On* neurons has the components summarized below and schematized in Fig. 2. The model parameters are listed in Table 1.

1. The model is a deterministic, integrate-to-threshold, point neuron whose operation is determined by an intracellular voltage and a threshold. The voltage change due to the flow of synaptic current through the neural membrane is represented by a parallel resistor-capacitor electrical circuit with a time constant, τ_m, equal to $R.C$. A spike discharge results when this membrane voltage exceeds a threshold, θ.

2. For a fixed refractory period, T_r, following a spike, the neuron cannot discharge again, so that the threshold is infinite and the membrane voltage is zero. Thus, we make no attempt to model the spike waveform, in order to improve computational efficiency. At the end of the refractory period T_r, the threshold is reset to its resting value, θ_0. T_r is always 0.7 ms in this article. It was chosen to correspond to the smallest interspike intervals observed in VCN neurons (e.g., Bourk, 1976; Young et al., 1988). These events are depicted in Fig. 3A, where the absolute refractory period is indicated by $\theta = \infty$.

Throughout the article, all voltages are expressed in units of the resting threshold, θ_0. With this normalization, θ takes two values, ∞ during refractory periods and the resting value of 1 in the remaining times.

3. All N synapses in the model are excitatory and driven by spikes from an equal number of independent model AN fibers (one fiber per synapse).

4. An input spike causes a transient increment in synaptic conductance, with a time course ("alpha function") described by

$$g_s(t) = G_s \frac{t}{\tau_s} \exp\left(-\frac{t}{\tau_s} + 1\right)$$

The synaptic time constant, τ_s, sets the duration of the conductance change; it is 0.1 ms for all synapses, resulting in a synaptic conductance change with a total duration of approximately 0.5 ms. This duration is consistent with measurements of synaptic currents from CN bushy cells (Isaacson and Walmsley, 1996). The magnitude of the conductance change, G_s, is also the same for all synapses.

In the article, G_s is always normalized by the unitary synaptic strength, G_0, which is the threshold amplitude of a synaptic conductance change that gives rise to a single output spike. This normalized synaptic strength is expressed by $G_\alpha = \frac{G_s}{G_0}$.[1] Model simulations show that G_0 is 0.189 mS when the membrane time constant, τ_m, has its default value of 0.125 ms and the parameters of the synapse model (τ_s and E/θ_0) are fixed to their values in Table 1.

5. There are between 1 and 2000 independent AN inputs to the model neuron. The CFs of these inputs are distributed on a log-frequency axis according to a Gaussian function. The mean of this function is defined as the characteristic frequency (CF) of the model *On* neuron. The standard deviation parameter of the Gaussian function is always 1/4 octave, giving a 1 octave *CF range* of the inputs for simulations of the leaky-integrator model in this article. It is an important parameter having substantial influence on entrainment, whose effect will be examined in detail in a future article. The choice of 1 octave in this article provides reasonable agreement between discharge characteristics of *On* neurons and discharge characteristics of the model, and it is generally consistent with the anatomy.

The CF of the model *On* neuron is 6000 Hz for all model simulations. We choose this value because actual *On* neurons tend to have high CFs.

6. Inputs to the model *On* neuron are exclusively model *high-spontaneous-rate AN fibers* because this AN population gives rise to the majority of AN synapses on many *On*-responding neurons (see the Discussion). These model AN fibers have a spontaneous discharge rate of 50 spikes/second.

Table 1 lists the parameters of the leaky-integrator model and indicates which ones are varied for the model simulations in this article.

2.3. Analytical Coincidence-Detector Model

We used an analytical coincidence-detector model to better understand the behavior of the *On* neuron leaky-integrator model. The model used here is similar in spirit to the binaural coincidence detector model of Colburn (1977).

The operation of this model can be understood in terms of a hypothetical intracellular potential. Each input spike during a fixed time window, Δt, increments the intracellular potential by a fixed positive amount, α. The increment due to each spike lasts throughout the duration of the time window. An output spike occurs when the intracellular potential exceeds a constant threshold. If the intracellular potential is normalized to the threshold or, equivalently, the threshold is set to 1, then α is analogous to the normalized synaptic strength, G_α, in the leaky-integrator model. (Note that α instead of G_α is used as a symbol for synaptic strength whenever the analytical coincidence-detector model is discussed.) There are N such synapses in the model driven by N independent inputs. Therefore, a spike is generated if at least n out of the N inputs have spikes on them within a given Δt, where

$$n = \frac{1}{\alpha}$$

This model has three parameters: N, α, and Δt. Whereas N and α are systematically varied in this article, Δt is fixed to 0.5 ms. This value roughly corresponds to the combined effect of the

---

[1]The effect of the synaptic reversal potential, E, is incorporated into the normalized synaptic strength. The precise value of E is not important so long as it is much greater than the threshold θ_0; this is the case for all model simulations in this study, where $E = 8.57 \cdot \theta_0$. When this condition is met, the increments in synaptic current due to an input spike are almost independent of the instantaneous value of the membrane voltage.

synaptic time constant, τ_s (0.1 ms), and the membrane time constant, τ_m (0.125 ms), of the leaky-integrator model.

If the N inputs to the coincidence-detector model are statistically independent, identically distributed Poisson processes[2] with rate $\lambda_{in}(t)$, then the probability of getting an output spike in a window of width Δt is given by binomial statistics:

$$p_{out}(t) = \sum_{i=n}^{N} \binom{N}{i} (\lambda_{in}(t)\Delta t)^i (1 - \lambda_{in}(t)\Delta t)^{(N-i)}.$$

(1)

The output spike train is approximately a Poisson process whose rate is

$$\lambda_{out}(t) = p_{out}(t)/\Delta t.$$

This expression for $\lambda_{out}(t)$ is studied as a function of N, α, and $\lambda_{in}(t)$ in Section 3.2. It should be noted that this model is limited by the absence of a refractory period and by the granularity of the time window Δt. This limitation prevents it from producing complex temporal discharge patterns such as those arising from phase-locking to low-frequency tones. Thus, the model is better suited for studying the transformation of input discharge rates to the output discharge rate than for investigating fine temporal patterns of discharge.

2.4. Characterization of Model Responses

We examine model discharge patterns in response to sound with PST histograms and interspike-interval histograms. Summary measures are extracted from these histograms for comparison with physiological data. We present typical values of these measures in model AN fibers together with the results of the leaky-integrator model and the analytical coincidence-detector model.

2.4.1. Shape of PST Histograms—All PST histograms plotted in the figures are constructed from model responses to 250 stimulus presentations, with the time-axis binned at 0.2 ms.

The type of PST histogram for high-frequency tone bursts is classified as either *On* or *Sustained* using the criteria of Winter and Palmer (1995). The criteria are based on a PST histogram for a 25 ms tone burst measured at 20 dB above CF tone-burst threshold, where threshold is the level at which the discharge rate exceeds the spontaneous rate by 10 spikes/second. The PST type is *On* if (1) the ratio of onset discharge rate to steady-state discharge rate is greater than 10 and (2) the steady-state rate is less than 50 spikes/sec; otherwise, the PST type is *Sustained*. The onset discharge rate is the rate of the largest 1 ms bin of the PST histogram, and the steady-state discharge rate is the discharge rate averaged over the last 12 ms of the 25 ms stimulus.

On PST histograms are further divided according to the criteria of Winter and Palmer (1995) into *On-I*, *On-L*, and *On-C* types based on the response to CF tone bursts at 50 dB above threshold. *On* PST histograms having two or more clearly defined onset peaks are *On-C*. *On* responses with no chopping are classified as *On-I* if the steady-state discharge rate is less than 10 spikes/second; otherwise, they are classified as *On-L*.

---

[2]Strictly speaking, the inputs are not Poisson because they are constrained to have at most one spike in the coincidence window; i.e., they have a dead time.

2.4.2. Entrainment Index—To determine the extent to which a response entrains to the stimulus, we define an entrainment index (*EI*) as the number of interspike intervals smaller than 1.5 stimulus periods divided by the number of stimulus cycles.[3]

EI quantifies a different aspect of the temporal discharge pattern than the commonly used synchronization index. The synchronization index quantifies the ability of a neuron to fire at a particular phase within a cycle of a periodic stimulus (Rose et al., 1967; Johnson, 1980). A neuron that is perfectly synchronized to the stimulus can nevertheless fail to entrain if it does not fire on every cycle of the stimulus.

3. Results

Our strategy is to first examine the conditions under which the leaky-integrator model has two key response properties of *On* neurons—a low spontaneous discharge rate and *On* PST histograms for high-frequency tone bursts. We then use a simple analytical coincidence detector model to get insight into the relationship between input and output discharge rates of the more complex computational model. Finally, we examine the characteristics that are needed for the computational model to entrain to low-frequency tones.

3.1. Spontaneous Discharge Rate and Responses to High-Frequency Tone Bursts for Leaky-Integrator Model

3.1.1. There is an Upper Bound on the Time Constant of the Leaky-Integrator Model for a Given Number of Inputs—Initially, we set the number of inputs, *N,* to 100 and the synaptic strength, G_α, to 1/20. These values are chosen because previous models show that many inputs and weak synapses help produce *On* PST histograms (Rothman et al., 1993; Kipke and Levy, 1997; Kalluri and Delgutte, 2001). With these parameters, we examine how spontaneous rate and PST histogram shape depend on the membrane time constant, τ_m. In the next section, we examine the effect of systematically varying *N* and G_α on spontaneous rate and PST histograms.

Spontaneous Rate: The effect of τ_m on spontaneous rate of the model can be understood by examining key variables of the model in Fig. 3A for $\tau_m = 1$ and $\tau_m = 4$ ms. The figures show the net synaptic current, membrane voltage, threshold, and spike times during a 100 ms segment of spontaneous activity. Even though the net synaptic strength is the same for the two cases, the membrane voltage is different. When $\tau_m = 4$ ms, the model acts as an integrator; it sums the contributions of many input spikes since the end of the previous absolute refractory period to generate the next output spike. In the limit of very large τ_m all input spikes sum (except for those occurring during absolute refractory periods), so the maximum output discharge rate is limited only by the refractory period. On the other hand, when $\tau_m = 1$ ms, many input spikes must occur in near coincidence for their voltage contributions to combine and lead to spikes. In the figure, there are too few such coincidences to cause spikes.

Figure 3B summarizes how the spontaneous rate of the model depends on τ_m in the range between 0.125 and 4 ms, approximately the range of membrane time constants in VCN neurons (Wu and Oertel, 1984; Golding et al., 1999). The grey-shaded region indicates the range of spontaneous rates for *On* neurons in the data (Godfrey et al., 1975b; Rhode and Smith, 1986). Spontaneous rate increases monotonically with τ_m, so that τ_m has to be small (<2 ms) for the model neuron to have a spontaneous rate (<2 spikes/sec) appropriate for *On* neurons.

---

[3]We use a different measure of entrainment than Joris et al. (1994b) because their measure does not distinguish between hyper-entraining responses and non-entraining responses. Joris et al. define the entrainment index as the number of intervals within a window 1 cycle wide and centered at 1 cycle on the abscissa of the interval histogram divided by the total number of interspike intervals. The short interspike intervals that occur in hyper-entraining responses are excluded by this definition, resulting in an entrainment index that is less than unity.

PST Histograms for High-Frequency Tone Bursts: As with spontaneous rate, the model produces PST histograms that are appropriate for *On* neurons when τ_m is small. Figure 4A and B show PST histograms for 6000 Hz (CF) tone bursts for two values of τ_m, 0.25 ms and 4 ms. When $\tau_m = 0.25$ ms, the shape of the PST histogram is *On*. In contrast, for $\tau_m = 4$ ms, the PST histogram is *Sustained*, with the onset peak smeared and the sustained rate too high. Figure 4C and D summarize how the shape of the PST histogram varies with τ_m. Figure 4C shows the ratio of onset rate to steady-state rate as a function of τ_m and D shows the steady-state discharge rate versus τ_m. In both panels, grey shading indicates the range appropriate for *On* neurons (as described in Methods). τ_m must be less than 0.5 ms for the model to produce *On* PST histograms. For larger τ_m, the onset peak gets smeared because it takes time to build up enough spikes on the inputs to trigger an output spike (Fig. 4B).

3.1.2. The Leaky-Integrator Model with a Small Time Constant Must Have Many AN Inputs Acting via Small Synapses—Based on the above findings, τ_m is set to a small value, 0.125 ms, in the rest of the article. In this section, we examine the effect of N and G_α on spontaneous rate and PST histograms.

Spontaneous Rate: The model readily produces low spontaneous rates appropriate for *On* neurons when N is large. To facilitate comparison of responses for different N, we use the *net synaptic strength*, $N \cdot G_\alpha$, instead of G_α to indicate strength of synapses. As a result, the net synaptic input is kept constant as N is varied. With this transformation, we cover the whole N versus G_α space, but in a way that gives more insight into their effects on response properties of the model. Figure 5 shows how spontaneous rate varies as a function of N and $N \cdot G_\alpha$. Spontaneous discharge rate in the *On* range (<2spikes/sec) is distinguished from excessive spontaneous rate (≥ 2 spikes/sec) with different symbols. For a fixed $N \cdot G_\alpha$, spontaneous rate decreases from above the *On* range to within this range as N increases. In the figure, the boundary between the two regions for spontaneous rate defines an iso-rate contour of 2 spikes/sec. This iso-rate contour deviates considerably from the horizontal, particularly for small N. This deviation means that the model can produce a low spontaneous rate in the *On* range even with a relatively large $N \cdot G_\alpha$ if N is sufficiently large, indicating that the net synaptic excitation alone does not predict the spontaneous rate; rather, spontaneous rate depends on both N and $N \cdot G_\alpha$.

These observations on the effect of N and $N \cdot G_\alpha$ apply equally well to steady-state rate for pure tones because, during the steady-state portion of pure tones, the discharge activity of the AN inputs is stationary like spontaneous activity. Because a low steady-state rate is a key factor for classifying a PST histogram as *On*, the shape of PST histograms for high-frequency tone bursts would be expected to depend on N and G_α in a similar way as spontaneous rate. This is what we show next.

PST Histograms for High-Frequency Tone Bursts: As with spontaneous rate, $N \cdot G_\alpha$ does not completely determine the shape of PST histograms for high-frequency tone bursts. Figure 6A, B, and C show PST histograms for CF (6000 Hz) tone bursts when N is equal to 10, 25, and 200, with $N \cdot G_\alpha$ held constant to 5. Increasing N from 10 to 25 results in the PST histogram shape changing from *Sustained* to *On* and further raising N to 200 accentuates the *On* shape of the PST histogram. Thus, PST histograms go from shapes similar to those of the AN inputs for small N to shapes that are very unlike those of AN inputs for large N. Additionally, increasing N to 200 allows the model to produce *On* PST histograms over a wider range of stimulus levels (not shown), or alternatively, across a broader range of $N \cdot G_\alpha$.

With different choices for N and $N \cdot G_\alpha$, the model can produce the three main types of *On* PST histogram in the VCN. Figure 6B, C, and D show *On-L*, *On-I*, and *On-C* PST histograms respectively. The model goes from producing *On-L* to *On-I* PST histograms as N is increased

because, as shown in the next section, the size of synaptic current decreases and causes fewer voltage crossings of the spike threshold. When $N \cdot G_\alpha$ and N are both large, the model produces *On-C* PST histograms, because immediately after the first spike, the synaptic current continues to be large enough to elicit additional spikes at stimulus onset just after the refractory period. These additional spikes underlie the chopping visible in the PST histogram. They tend to be spaced evenly because the fluctuations of the synaptic current are small due to the large N.

Figure 7 shows how PST shape for 6000 Hz tone bursts depends on both $N \cdot G_\alpha$ and N. The model response has an *On* PST shape for increasingly larger values of $N \cdot G_\alpha$ as N increases. The boundary between the regions of *On* PST histograms and *Sustained* PST histograms is not horizontal. Therefore, $N \cdot G_\alpha$ alone does not predict PST shape. As with spontaneous rate, both synaptic strength and number of inputs are needed to predict PST shape in the model.

The requirements of small τ_m and large N tradeoff against each other. For a given $N \cdot G_\alpha$, τ_m does not have to be quite so small to produce *On* PST histograms and low spontaneous rate if N is large. Nevertheless, because N cannot be more than the 500 to 600 AN inputs of *On* neurons (see the Discussion), there is an absolute upper bound on τ_m, such that it must be small (≤ 0.5 ms) to produce *On* PST histograms and low spontaneous rates.

3.2. Understanding the Behavior of The Leaky-Integrator Model with an Analytical Coincidence-Detector Model

In this section, we examine the extent to which the transformation of input discharge rates to output discharge rates in the leaky-integrator model resembles the transformation by a coincidence detector. We determine how spontaneous rate and PST histogram shape depend on the number of inputs and synaptic strength in the analytical coincidence-detector model and compare these results with those for the leaky-integrator model.

3.2.1. Spontaneous Rate—Equation (1) can be used to look at the spontaneous rate and the PST histograms for CF tone bursts in the *analytical* coincidence-detector model. The equation gives the smoothed instantaneous discharge rate, $\lambda_{out}(t)$, in terms of the discharge rates of the inputs, $\lambda_{in}(t)$, the number of independent inputs, N, and the strength of synapses, α.

A meaningful way of assessing the effect of N on λ_{out} is to vary N while holding the net synaptic strength, $N \cdot \alpha$, constant because the expected value of the intra-cellular voltage in the analytical model, $\bar{v}(t)$, is directly proportional to $N \cdot \alpha$. Specifically, with the assumptions of the analytical model presented in the Methods section and with λ_{in} fixed, $\bar{v}(t)$ is given by

$$\bar{v}(t) = N \cdot \alpha \cdot \lambda_{in}(t) \cdot \Delta t. \tag{2}$$

If the discharge rate of the analytical model were proportional to $\bar{v}(t)$, then $\lambda_{out}(t)$ would depend only on $N \cdot \alpha$. In other words, if $N \cdot \alpha$ is held constant, then discharge rate should not change as N is varied. However, Fig. 8 shows that when $N \cdot \alpha$ is held constant and λ_{in} is fixed to 50 spikes/sec (the spontaneous rate of the model AN inputs), the response of the analytical model decreases with N. As was the case with spontaneous rate in the leaky-integrator model, the spontaneous rate of the analytical model can be in the range for *On* neurons (<2 spikes/sec) even for relatively large $N \cdot \alpha$ if there are a large number of inputs.

$N \cdot \alpha$ does not predict the spontaneous rate by itself because the intracellular voltages that lead to the discharge rates of Fig. 8 are in the regime where $\bar{v} \ll 1$. Thus, $\bar{v}$ by itself is always below threshold and spikes are caused only by voltage fluctuations.[4] However, whereas $\bar{v}$ grows with N (for fixed α), the fluctuations, σ_v in Eq. (3), grow with $\sqrt{N}$—that is, the fluctuations grow more slowly with N than does $\bar{v}$.

$$\sigma_\upsilon(t) = \frac{N \cdot \alpha}{\sqrt{N}} \sqrt{\lambda_{in}(t)\Delta t(1 - \lambda_{in}(t)\Delta t)}$$

(3)

Therefore, when the mean voltage is held constant by fixing $N \cdot \alpha$, the voltage fluctuations decrease with increasing N. As a result, there are fewer threshold crossings and consequently lower discharge rates.

3.2.2. PST Histograms for High-Frequency Tone-Bursts—The reduction of fluctuations with increasing N affects the shape of PST histograms produced by the analytical model. Figure 9 shows how the voltage of the analytical model varies with N for a 6000 Hz tone burst. The intracellular voltage at onset becomes increasingly distinct from that in the sustained part because the voltage fluctuations get smaller as N is increased. Therefore, when N is large, a threshold can be chosen such that the analytical model produces spikes at the onset but not the steady-state part of the tone burst.

The effect of N on PST shape in the analytical model is examined directly with the aid of Eq. (1) which relates $\lambda_{out}(t)$ to $\lambda_{in}(t)$. Because the PST histograms are estimates of instantaneous rates $\lambda_{out}(t)$ and $\lambda_{in}(t)$, the equation gives an exact expression relating the smoothed output PST histogram to the smoothed PST histogram of the inputs.

The reduction in voltage fluctuations with increasing N causes the relationship between $\lambda_{out}(t)$ and $\lambda_{in}(t)$ to become increasingly threshold-like. Figure 10A shows the input-output relation of the analytical model for N equal to 1, 25, 100, and 400, with $N \cdot \alpha$ fixed. The main effect of increasing N is to increase the slope of the input-output function. As a result, for large N, there is a threshold effect in the relationship between output and input.

The threshold effect in the input-output relation for large N results in the *Sustained* PST histograms on the inputs being transformed into *On* PST histograms. Figure 10B shows how this effect occurs for a 60 dB SPL, 6000 Hz tone burst by comparing the PST histogram for $N = 400$ with the PST histogram for $N = 1$. For $N = 1$, the input-output relation is linear with a slope of 1 and therefore, the output PST histogram is the same as the input PST histogram. In contrast, for $N = 400$, the threshold effect in the relationship between $\lambda_{out}(t)$ and $\lambda_{in}(t)$ amplifies the high discharge rate at onset and severely reduces the steady-state rate, resulting in an *On* PST histogram. It is clear from this input-output relationship that the tone-burst response of the AN inputs must be greater at the stimulus onset than during the steady-state for the model to produce *On* PST histograms.

Figure 11 summarizes the shape of the output PST histogram as a function of $N \cdot \alpha$ and N. The similarity with the corresponding plot for the leaky-integrator model in Fig. 7 confirms that the leaky-integrator model resembles a coincidence detector under the conditions for which it produces realistic *On* PST histograms for high-frequency tones.

3.2.3. Summary of Modeling *On* PST Histograms for High-Frequency Tone Bursts—In summary, it is possible to account for *On* PST histograms for high-frequency tone bursts using a leaky-integrator model with a small time constant (<0.5 ms) and a large number of inputs (>80). Although *On* PST histograms and low spontaneous rates can also be obtained with fewer inputs, the range of synaptic strengths and stimulus levels over which these properties hold is much more restricted. The similarity between a leaky-integrator and a coincidence detector in how the PST histogram shape depends on the number of inputs and

---

[4]When $\bar{\upsilon} \gg 1$, the spontaneous rate is determined by intrinsic membrane properties. For example, in a neuron having refractoriness, the spontaneous rate would be limited by the refractory period. Since the analytic model has no such refractoriness, the spontaneous rate is limited by Δt, the width of the coincidence window.

the strength of synaptic connections suggests that the leaky-integrator model transforms discharge rates of its inputs into outputs similarly to a coincidence detector. Given that the analytic coincidence detector is not suitable for examining fine temporal patterns of discharge (see the Methods section), we examine responses to low-frequency tones below only with the leaky-integrator model.

3.3. Entrainment to Low-Frequency Tones

The remarkable feature of entrainment to low-frequency stimuli by *On* neurons is that it typically occurs for frequencies up to 800 Hz, but as high as 1000 Hz in some neurons (Rhode and Smith, 1986). Furthermore, these same *On* neurons do not hyper-entrain (fire more than 1 spike per cycle) to very low frequencies (e.g., below 300 Hz). Entrainment to tone frequencies greater than 700 to 800 Hz is remarkable because the resulting interspike intervals are close to the lower limit set by the absolute refractory period of neurons. In this section, we show that the leaky-integrator model can entrain to low-frequency tones while giving *On* PST histograms for high-frequency tone bursts. However, the model cannot do so without chopping at stimulus onset for high-frequency tone bursts; i.e., the model is most appropriate for *On-C* neurons.

3.3.1. The Leaky-Integrator Model Entrains to Low-Frequency Tones Over a Limited Range of Frequencies—In contrast to *On* neurons, AN fibers do not entrain to low-frequency tones. Indeed, the dashed curve in Fig. 12A shows that a model AN fiber with a CF of 6000 Hz, produces entrainment indices (*EI*s) far less than 1 for a broad range of low-frequency tones.

The leaky-integrator model enhances the entrainment present in the model AN fibers across a broad range of frequencies. The solid line in Fig. 12A shows entrainment as a function of frequency for the leaky-integrator model. The model has a short membrane time constant ($\tau_m = 0.125$ ms) and many inputs ($N = 400$), with net synaptic strength ($N \cdot G_\alpha = 8.8$) chosen such that the PST histograms for high-frequency tone bursts are *On*. For frequencies between 400 Hz and 800 Hz, the model entrains to the stimulus ($EI \approx 1$). Above this frequency range, the model fails to entrain while below this frequency range, the model hyper-entrains ($EI > 1$).

The almost perfect entrainment between 400 Hz and 800 Hz is evident in histograms of intervals between consecutive spikes ("interval histograms") in Fig. 12B; for example, the interval histogram for an 800 Hz tone shows that almost all intervals are equal to 1.25 ms, the stimulus period. Above this frequency range, for example at 1000 Hz, the model fails to entrain because spikes do not occur on every stimulus cycle. For these high frequencies the model is unable to recover quickly enough after a spike to fire again in the next stimulus cycle. Below the frequency range for entrainment, the model hyper-entrains ($EI > 1$). The interval histogram for a 200 Hz tone shows that hyper-entrainment results from the insertion of intervals shorter than the 5 ms stimulus period. The shortest intervals are close to the absolute refractory period ($T_r = 0.7$ ms). There are also some intervals with a duration of 4.3 ms, which is the difference between the stimulus period and T_r. At the hyper-entrainment frequencies, the model produces a spike early enough during a stimulus cycle to recover and produce another spike.

In general, the pattern of intervals at each frequency is determined by the interaction between the synaptic current waveform and the characteristics of the recovery after a spike. Thus, although the minimum recovery time after a spike is set by T_r, the actual recovery time is determined by the size of the synaptic current as well as the membrane time constant (τ_m) and the synaptic time constant (τ_s).

In Fig. 13A, with *N* fixed to 400, the strength of synapses, G_α, is lowered from that in Fig. 12 to see if the leaky-integrator model can still entrain to tones up to 800 Hz without also hyper-entraining to very low-frequency tones. The idea is that, with lower G_α, the synaptic current

may be sufficiently small that the recovery after a spike is not rapid enough to permit a second spike during a given stimulus cycle. Indeed, the figure shows that when $N \cdot G_\alpha$ is lowered from 8.8 to 7.5, the model no longer hyper-entrains to tones less than 400 Hz. However, while hyper-entrainment is eliminated, the upper frequency limit for entrainment falls from 800 Hz to 600 Hz. Further lowering $N \cdot G_\alpha$ to 5 results in a failure of the model to entrain to tones of any frequency. The frequency range for entrainment never exceeds approximately 400 Hz, so that it is not possible to get entrainment to both high frequencies (≥800 Hz) and low frequencies (<400 Hz) by varying the net synaptic input.

The response properties of the leaky-integrator model, when $N \cdot G_\alpha = 7.5$, are consistent with those of *On-C* neurons. The model entrains over a 400 Hz range of frequencies without hyper-entraining to low frequencies and furthermore, it produces *On-C* PST histograms for 6000 Hz tone bursts (Fig. 13C). *On-C* neurons with such a combination of properties have been reported (Rhode and Smith, 1986). Chopping in the PST histogram occurs because the synaptic input is large enough at stimulus onset to enable the model to fire again after the first spike.

While the model can produce entrainment and PST histograms appropriate for *On-C* neurons, it cannot simulate both entrainment and PST histograms of *On-I/L* neurons. *On-I* and *On-L* neurons also entrain to a broad range of frequencies but produce *On* PST histograms without chopping. Reducing $N \cdot G_\alpha$ to 5 results in an *On* PST histogram that does not have chopping (Fig. 13D), but then the model fails to entrain at all (Fig. 13A). There is therefore a tradeoff between the ability of the model to entrain over a broad range of frequencies and its ability to produce *On* PST histograms without chopping.

3.3.2. The Effect of the Number of Inputs—We also examined whether a large number of inputs, *N,* might enable the leaky-integrator model to produce both *On* PST histograms lacking chopping and realistic entrainment. A very large number of inputs may help because changing *N* in the model reduces the steady-state discharge rate for high-frequency tone bursts but does not greatly alter entrainment to low-frequency tones. Indeed, the frequency range of entrainment in the model is not greatly affected by the number of inputs for $N \geq 100$ (not shown). This occurs because changing *N,* while $N \cdot G_\alpha$ is fixed, alters the variability without altering the mean probability of firing. At low frequencies, the difference between the crest and valley of the probability of firing is large, so that altering the variability does not greatly change entrainment. As for responses to high-frequency tone bursts, increasing *N* to as high a value as 2000 extinguishes the steady-state response but fails to eliminate chopping (not shown). Thus, even with a very large number of inputs, the model is unable to produce both entrainment to a broad range of low-frequency tones and *On* PST histograms without chopping for high-frequency tone bursts.

4. Discussion

4.1. *On* Discharge Patterns Produced by the Leaky-Integrator Model

Our results indicate that the leaky-integrator model produces *On* PST histograms and entrainment when it has a small membrane time constant, τ_m (0.125 ms), and a large number of inputs, *N* (>100), so as to act like a coincidence detector. However, because it cannot entrain to a broad range of frequencies without also chopping at the onset of high-frequency tone bursts, the leaky-integrator model is appropriate only for *On-C* neurons. The relationship of the frequency range of entrainment and PST histogram shape to *N* in the leaky-integrator model leads to a prediction for *On-C* neurons that can be tested experimentally. Namely, because the frequency range of entrainment increases with *N* and steady-state discharge rate declines with *N* (Figs. 6 and 7) in the leaky-integrator model, one should observe an inverse relationship between frequency range of entrainment and steady-state discharge rate.

Although we have focused on PST histogram shape and entrainment, two other response properties have been examined extensively in experiments—the standard deviation of first-spike latency for high-frequency tone bursts and phase-locking to low-frequency tones. The standard deviation of first-spike latency in *On* neurons is amongst the smallest of all CN neurons (Rhode and Smith, 1986; Young et al., 1988; Winter and Palmer, 1995). Phase-locking to low-frequency tones in *On* neurons (<1000 Hz) is enhanced relative to that in AN fibers (Godfrey et al., 1975b; Bourk, 1976; Rhode and Smith, 1986, Blackburn and Sachs, 1989, Joris et al., 1994b, 1994a). With parameters that result in *On* PST histograms and entrainment, the leaky-integrator model also produces enhanced phase-locking and a small standard deviation of first spike latency. We have not presented these results because these response properties are less sensitive to model parameters than are entrainment and PST histogram shape. Earlier modeling studies have also noted that the jitter in spike timing is greatly reduced when a large number of inputs converge onto a neuron (Marsalek et al., 1997; Burkitt and Clark, 1999; Banks and Sachs, 1991) and that enhancement of phase-locking results from the convergence of independent synaptic inputs (Banks and Sachs, 1991; Joris et al., 1994b; Rothman and Young, 1996).

4.2. Relation to Experimental Findings

In general, the parameters of the leaky-integrator model that produce realistic *On* response properties are consistent with anatomical observations from octopus cells and D-stellate cells, which are putative *On*-responding neurons (Godfrey et al., 1975b; Rhode et al., 1983; Rouiller and Ryugo, 1984; Smith and Rhode, 1989). These neurons have a large number of synapses, all of which are small (Smith and Rhode, 1989; Liberman, 1991, 1993; Ostapoff et al., 1994; Golding et al., 1995). Liberman (1993) estimates that octopus cell somata receive approximately 60 synapses from the AN, a smaller number than the 100 inputs required by the model to get realistic *On* discharge patterns. However, Liberman's estimate includes only synapses on the soma, yet both octopus cells and D-stellate cells receive synaptic input from the AN on their dendrites as well (Kane, 1973; Brawer et al., 1974; Smith and Rhode, 1989). Based on measurements of somatic and dendritic surface areas, fractions of the surface areas occupied by the synaptic contacts, and the average surface areas of the synaptic contacts in octopus cells and D-stellate cells (Kane, 1973; Smith and Rhode, 1989), we estimate 500 to 600 AN synapses per cell for these cell types, consistent with our prediction. Moreover, our finding that increasing the number of inputs (with net synaptic input held constant) reduces discharge rate is consistent with (and an explanation of) the similar reduction of discharge rate observed in binaural coincidence-detecting neurons of barn owl nucleus laminaris *in vitro* for current injections simulating increasing numbers of synaptic inputs (Reyes et al., 1996).

Our prediction that the inputs must be weak is consistent with anatomical observations that individual synapses are small relative to the size of the cell (Kane, 1973; Smith and Rhode, 1989; Liberman 1991, 1993; Ostapoff et al., 1994; Golding et al., 1995). Furthermore, the amplitude of excitatory postsynaptic potentials recorded from octopus cells *in vitro* rises in very small increments in response to shocks of the AN of progressively increasing strength, suggesting that each AN input has a weak post-synaptic effect (Golding et al., 1995).

Intracellular recordings from octopus cells and other *On*-responding cells *in vitro* (Wu and Oertel, 1984; Oertel, et al., 1990; Golding et al., 1995, 1999) are consistent with the model prediction that *On* neurons must have small membrane time constants. For example, the membrane time constant of octopus cells near the resting voltage is between 0.2 and 0.4 ms (Golding et al., 1999). In fact, the time constant may effectively be even lower during synaptic excitation due to activation of synaptic conductances and voltage-dependent conductances, such as the low-threshold potassium channel found in bushy cells and octopus cells (Manis and Marx, 1991; Golding et al., 1995, 1999).

The models in our study are most applicable to *On* neurons whose responses to high-frequency tone bursts have a sharply timed first spike and which entrain to low-frequency tones. A small number of *On* neurons have been observed in the AVCN (Bourk, 1976) and DCN (Godfrey et al., 1975a) whose PST histograms do not have such sharply timed first spikes and which do not entrain nor phase-lock very well to low-frequency tones. The *On* neurons in Bourk (1976) were mostly in the edges of the anterior AVCN, a region that differs from the core regions of the VCN in its proportionally greater innervation from high-threshold low-spontaneous-rate AN fibers compared to innervation from low-threshold high-spontaneous-rate AN fibers (Liberman, 1991). It may be possible to modify the leaky-integrator model to account for the discharge patterns of these other *On* neurons, for instance by reducing the number of inputs, increasing the membrane time constant, and including low-spontaneous-rate AN inputs. Nevertheless, the *On* neurons that are most relevant to our study are from the core regions of the VCN, mainly the posterior AVCN and PVCN (Godfrey et al., 1975b; Blackburn and Sachs, 1989; Jiang et al., 1996).

4.3. Simplifying Assumptions

We left out several known features of *On* neurons in the leaky-integrator model. Specifically, there were three important simplifying assumptions: (1) *On* neurons can be modeled as point neurons, (2) there are only high-spontaneous-rate AN inputs, and (3) there are no inhibitory inputs.

The assumption of a point neuron (i.e., spatial variations of membrane voltage within a cell are negligible) is well supported by observations from *On* neurons, including morphology (Rhode et al., 1983; Rouiller and Ryugo, 1984; Smith and Rhode, 1987, 1989; Ostapoff et al., 1994) that is characteristic of point neurons (Weiss, 1995), short electrotonic length of dendrites estimated from compartmental models (Levy and Kipke, 1997; Cai et al., 1997), and brief miniature synaptic currents showing little evidence of dendritic filtering (Gardner et al., 1999). The assumption of exclusively high-spontaneous-rate AN inputs to the leaky-integrator model is justified by the observation that some *On* neurons (e.g., octopus cells and globular bushy cells) appear to get few inputs from low- and medium-spontaneous-rate AN fibers (Liberman, 1991, 1993).

As for the absence of synaptic inhibition, this assumption holds only for a subset of *On* neurons. Recent experiments with iontophoretic injection of bicuculline, a GABA-A receptor antagonist, suggest that inhibitory inputs shape the response properties of *On-L* and *On-C* neurons (*On-I* neurons do not appear to get substantial inhibition) (Palombi and Caspari, 1992; Evans and Zhao, 1997). However, too little is known about the origin and properties of these inputs to develop a model that includes them. Nevertheless, inhibition is unlikely to help the leaky-integrator model produce both entrainment over a broad frequency range and *On* PST histograms lacking chopping. The effect of sustained inhibition should be equivalent to decreasing the strength of synapses, which could eliminate onset chopping but would reduce the frequency range of entrainment as well. Short-latency inhibition that is time-locked to the excitation on a cycle-per-cycle basis (Grothe and Park, 1998) is not likely to help either because inhibitory post-synaptic potentials in the CN tend to be long (4 to 10 ms in stellate cells and bushy cells) (Oertel, 1983); such long synaptic potentials would be expected to reduce the upper frequency limit of entrainment.

In summary, we have made several simplifying assumptions that are generally consistent with known properties of *On* neurons. The assumption of no inhibitory inputs is no doubt valid only to a limited extent in many *On* neurons. Nevertheless, it is convenient to make this assumption because the number of parameters in the model is kept to a minimum, allowing us to thoroughly explore the parameter space and make testable predictions.

4.4. Models for Subtypes of *On* Neurons That Lack Chopping

Our analytical coincidence-detector model confirms past hypotheses that a coincidence-detection mechanism can produce *On* discharge patterns when fed with an adapting PST histogram (Rhode and Smith, 1986; Kim et al., 1986; Joris et al., 1994b; Golding et al., 1995; Evans, 1998). We have shown that *On* PST histograms result in the analytical model from a threshold effect in the instantaneous relationship between the input discharge rate and the output discharge rate for a large number of inputs. The threshold effect enhances the rapid onset discharge rate and reduces the lower steady-state discharge rate of the AN inputs. We have further shown that a coincidence detector combined with a conventional refractory mechanism, as in our leaky-integrator model, is not sufficient to account for discharge patterns of all types of *On* neurons—specifically, *On* neurons that do not chop (*On-I/L* neurons).

In order to produce *On-I* and *On-L* discharge characteristics, a model must prevent short interspike intervals from occurring during high-frequency tone bursts but must allow them during low-frequency tones in order to entrain. These opposing constraints cannot be achieved by the leaky-integrator model, which either permits or prevents short interspike-intervals for all stimuli.

The conclusion that the leaky-integrator model cannot produce both *On-I/L* PST histograms for high-frequency tone bursts and entrainment over a wide range of frequencies also applies to broader classes of models. For example, models that combine a conventional absolute refractory period with an accommodative threshold do not appear to work (Kalluri, 2000). Such models produce *On* PST histograms for high-frequency tone bursts more readily than does the leaky-integrator model with no accommodation (i.e., over a wider range of stimulus levels and a wider range of synaptic strengths) (Arle and Kim, 1991; Evans, 1998; Kalluri and Delgutte, 2001). Accommodation is a phenomenological concept that has been used for modeling the effects of low-threshold voltage-dependent potassium currents on membrane voltage (Rashevsky, 1933; Monnier, 1934; Hill, 1936). An accommodative threshold is a low-pass filtered version of the membrane voltage. Because comparison of membrane voltage to a threshold is a form of subtraction, accommodation effectively acts like a high-pass filter that emphasizes transients in the synaptic current. This high-pass filtering effect enables models with accommodative thresholds to readily produce transient responses at the onset of high-frequency tone bursts. Nevertheless, such models still fail to produce both entrainment to a broad range of frequencies and *On-I/L* PST histograms. The failings of the accommodation models are the same as those of the leaky-integrator model with no accommodation. Interspike intervals can be constrained to be either large or small for both high-frequency tone bursts and low-frequency tones, but not different for the two stimuli.

Broader classes of models that will not work are those that behave like the non-stationary renewal processes used to model AN fibers (Johnson and Swami, 1983). In these processes, the probability of spiking is a separable product of a function of the time since the previous spike (intrinsic neuronal properties including refractoriness) and a function of the stimulus. Such models will fail because the separability of refractory effects and stimulus-dependent effects prevents the lower limit on interspike intervals from changing with the stimulus.

In this article, we have shown that a leaky-integrator model can produce *On-I*, *On-L*, and *On-C* PST histograms for different number of inputs and synaptic strengths. Because the model produces *On-I/L* PST histograms only when the net synaptic input is small, it fails to simultaneously, entrain to a broad range of low-frequency tones. In the second article, of our series, we modify the leaky-integrator model to produce both *On-I/L* PST histograms and entrainment.

References

Arle J, Kim D. Neural modeling of intrinsic and spike-discharge properties of cochlear nucleus neurons. Biol Cyber 1991;64:273–283.

Banks M, Sachs M. Regularity analysis in a compartmental model of chopper units in the anteroventral cochlear nucleus. J Neurophys 1991;65:606–629.

Blackburn C, Sachs M. Classification of unit types in the anteroventral cochlear nucleus: PST histograms and regularity analysis. J Neurophys 1989;62(6):1303–1329.

Bourk, T. Ph.D. dissertation. Massachusetts Institute of Technology; 1976. Electrical responses of neural units in the anteroventral cochlear nucleus of the cat.

Brawer J, Morest D, Kane E. The neuronal architecture of the cochlear nucleus of the cat. J Comp Neurol 1974;155:251–300. [PubMed: 4134212]

Bregman, AS. Auditory Scene Analysis. MIT Press; Cambridge, MA: 1990.

Burkitt AN, Clark GM. Analysis of integrate-and-fire neurons: Synchronization of synaptic input and spike output. Neural Comput 1999;11(4):871–901. [PubMed: 10226187]

Cai Y, Walsh EJ, McGee J. Mechanisms of onset responses in octopus cells of the cochlear nucleus: Implications of a model. J Neurophys 1997;78:872–883.

Cai Y, Walsh EJ, McGee J. Contributions of ionic conductances to the onset responses of octopus cells in the ventral cochlear nucleus. J Neurophys 2000;83(1):301–314.

Cant, N. The cochlear nucleus: Neuronal types and their synaptic organization. In: Webster, DB.; Popper, AN.; Fay, RR., editors. The Mammalian Auditory Pathway: Neuroanatomy. Springer-Verlag; New York: 1992. p. 66-116.

Cant N, Morest D. Organization of the neurons in the anterior division of the anteroventral cochlear nucleus of the cat: Light-microscopic observations. Neuroscience 1979;4:1909–1923. [PubMed: 530438]

Carney L. A model for the responses of low-frequency auditory-nerve fibers in cat. J Acoust Soc Am 1993;93:401–417. [PubMed: 8423257]

Colburn H. Theory of binaural interaction based on auditory-nerve data: II. Detection of tones in noise. J Acoust Soc Am 1977;61:525–533. [PubMed: 845314]

de No, RL. The Primary Acoustic Nuclei. Raven Press; New York: 1981.

Deutsch, D. The Psychology of Music. Academic Press; New York: 1982.

Eriksson JL, Robert A. The representation of pure tones and noise in a model of cochlear nucleus neurons. J Acoust Soc Am 1999;106(4):1865–1879. [PubMed: 10530012]

Evans, EF. Modeling characteristics of Onset-I cells in guinea pig cochlear nucleus. In: Greenberg, S.; Slaney, M., editors. Proceedings of the NATO Advanced Study Institute on Computational Hearing. Il Ciocco (Tuscany); Italy. 1998. p. 1-6.

Evans, EF.; Zhao, W. Periodicity coding of the fundamental frequency of harmonic complexes: Physiological and pharmacological study of onset units in the ventral cochlear nucleus. In: Palmer, AR.; Rees, A.; Summerfield, AQ.; Meddis, R., editors. Psychophysical and Physiological Advances in Hearing. Whurr; London: 1997. p. 186-194.

Frisina R, Smith R, Chamberlain S. Encoding of amplitude modulation in the gerbil cochlear nucleus: I. A hierarchy of enhancement. Hear Res 1990;44:99–122. [PubMed: 2329098]

Gardner S, Trussell L, Oertel D. Time course and permeation of synaptic AMPA receptors in cochlear nucleus neurons correlate with input. J Neurosci 1999;19:8721–8729. [PubMed: 10516291]

Godfrey D, Kiang N, Norris B. Single unit activity in the dorsal cochlear nucleus. J Comp Neurol 1975a; 162:269–284. [PubMed: 1150922]

Godfrey D, Kiang N, Norris B. Single unit activity in the posteroventral cochlear nucleus. J Comp Neurol 1975b;162:247–268. [PubMed: 1150921]

Golding NL, Ferragamo MJ, Oertel D. Role of intrinsic conductances underlying responses to transients in octopus cells of the cochlear nucleus. J Neurosci 1999;19(8):2897–2905. [PubMed: 10191307]

Golding NL, Robertson D, Oertel D. Recordings from slices indicate that octopus cells of the cochlear nucleus detect coincident firing of AN fibers with temporal precision. J Neurosci 1995;15:3138–3153. [PubMed: 7722652]

Grothe B, Park TJ. Sensitivity to interaural time differences in the medial superior olive of a small mammal, the Mexican free-tailed bat. J Neurosci 1998;18(16):6608–6622. [PubMed: 9698347]

Hill AV. Excitation and accomodation in nerve. Proc Roy Soc (London), Ser B 1936;119:305–355.

Isaacson JS, Walmsley B. Amplitude and time course of spontaneous and evoked excitatory postsynaptic currents in bushy cells of the anteroventral cochlear nucleus. J Neurophys 1996;76:1566–1571.

Jiang D, Palmer A, Winter IM. Frequency extent of two-tone facilitation in onset units in the ventral cochlear nucleus. J Neurophys 1996;75:380–395.

Johannesma, PIM. The pre-response stimulus ensemble of neurons in the cochlear nucleus. Proceedings of the Symposium on Hearing Theory; IPO, Eindhoven, The Netherlands. 1972. p. 58-69.

Johnson D. The relationship between spike rate and synchrony in responses of auditory-nerve fibers to single tones. J Acoust Soc Am 1980;68(4):1115–1122. [PubMed: 7419827]

Johnson D, Swami A. The transmission of signals by auditory-nerve fiber discharge patterns. J Acoust Soc Am 1983;74(2):493–501. [PubMed: 6311884]

Joris P, Smith P, Yin T. Enhancement of neural synchronization in the anteroventral cochlear nucleus. II. Responses in the tuning curve tail. J Neurophys 1994a;71:1037–1051.

Joris PX, Carney L, Smith P, Yin T. Enhancement of neural synchronization in the anteroventral cochlear nucleus: I. Responses to tones at the characteristic frequency. J Neurophys 1994b;71:1022–1036.

Kalluri, S. Ph.D. dissertation. Massachusetts Institute of Technology; 2000. Cochlear nucleus onset neurons studied with mathematical models.

Kalluri, S.; Delgutte, B. A general model of spiking neurons applied to onset responders in the cochlear nucleus. 1996 Computational Neurosciences Conference; 1996.

Kalluri S, Delgutte B. An electrical circuit model for cochlear nucleus onset responders. Assoc Res Otolaryngol Abstr 1997;20:456.

Kalluri, S.; Delgutte, B. Characteristics of cochlear nucleus onset units studied with a model. In: Greenberg, S.; Slaney, M., editors. Computational Models of Auditory Function. IOS Press; Amsterdam: 2001.

Kane EC. Octopus cells in the cochlear nucleus of the cat: Heterotypic synapses upon homeotypic neurons. Intern J Neuroscience 1973;5:251–279.

Kiang, N.; Morest, D.; Godfrey, D.; Guinan, J.; Kane, E. Stimulus coding at caudal levels of the cat's auditory system: I. Response characteristics of single units. In: Moller, AR., editor. Basic Mechanisms in Hearing. Academic Press; New York: 1973. p. 455-478.

Kiang, N.; Watanabe, T.; Thomas, E.; Clark, L. Discharge Patterns of Single fibers in the Cat's Auditory Nerve. MIT Press; Cambridge, MA: 1965.

Kim, D.; Rhode, W.; Greenberg, S. Responses of cochlear nucleus neurons to speech signals: Neural encoding of pitch, intensity, and other parameters. In: Moore, B.; Patterson, R., editors. Auditory Frequency Selectivity. Plenum Press; New York: 1986. p. 281-288.

Kim DO, Sirianni JG, Chang SO. Responses of DCN-PVCN neurons and auditory nerve fibers in unanesthetized decerebrate cats to AM and pure tones: Analysis with autocorrelation/power spectrum. Hearing Research 1990;45:95–113. [PubMed: 2345121]

Kipke DR, Levy KL. Sensitivity of the cochlear nucleus octopus cell to synaptic and membrane properties: A modeling study. J Acoust Soc Am 1997;102:403–412.

Levy K, Kipke D. Mechanisms of the cochlear nucleus octopus cell's onset response: Synaptic effectiveness and threshold. J Acoust Soc Am 1998;103:1940–1950. [PubMed: 9566317]

Levy KL, Kipke DR. A computational model of cochlear nucleus octopus cell. J Acoust Soc Am 1997;102:391–402.

Liberman MC. Central projections of auditory-nerve fibers of differing spontaneous rate: I. Anteroventral cochlear nucleus. J Comp Neurol 1991;313:240–258. [PubMed: 1722487]

Liberman MC. Central projections of auditory-nerve fibers of differing spontaneous rate: II. Posteroventral and dorsal cochlear nucleus. J Comp Neurol 1993;327:17–36. [PubMed: 8432906]

Manis P, Marx S. Outward currents in isolated ventral cochlear nucleus neurons. J Neurosci 1991;11:2865–2880. [PubMed: 1880553]

Marsalek P, Koch C, Maunsell J. On the relationship between synaptic input and spike output jitter in individual neurons. Proc Natl Acad Sci USA 1997;94(2):735–740. [PubMed: 9012854]

Monnier, A. L'Excitation Electrique des Tissus. Hermann; Paris: 1934.

Morest, D.; Kiang, N.; Kane, E.; Guinan, J.; Godfrey, D. Stimulus coding at caudal levels of the cat's auditory system: II. Patterns of synaptic organization. In: Moller, AR., editor. Basic Mechanisms of Hearing. Academic Press; New York: 1973. p. 479-509.

Oertel D. Synaptic responses and electrical properties of cells in brain slices of the mouse anteroventral cochlear nucleus. J Neurosci 1983;3:2043–2053. [PubMed: 6619923]

Oertel D, Wu SH, Garb M, Dizack C. Morphology and physiology of cells in slice preparations of the posteroventral cochlear nucleus of mice. J Comp Neurol 1990;295:136–154. [PubMed: 2341631]

Ostapoff E-M, Feng J, Morest D. A physiological and structural study of neuron types in the cochlear nucleus: II. Neuron types and their structural correlation with response properties. J Comp Neurol 1994;346:19–42. [PubMed: 7962710]

Palombi P, Caspari D. GABAa receptor antagonist bicuculline alters response properties of posteroventral cochlear nucleus neurones. J Neurophys 1992;67:738–746.

Pfeiffer R. Classification of response patterns of spike discharges for units in the cochlear nucleus: Tone-burst stimulation. Exp Brain Res 1966;1:220–235. [PubMed: 5920550]

Rashevsky N. Outline of a physico-mathematical theory of excitation and inhibition. Protoplasma 1933;20:42–56.

Reyes AD, Rubel EW, Spain WJ. *In vitro* analysis of optimal stimuli for phase-locking and time-delayed modulation of firing in avian nucleus laminaris neurons. J Neurosci 1996;16(3):993–1007. [PubMed: 8558268]

Rhode W, Greenberg S. Encoding of amplitude modulation in the cochlear nucleus of the cat. J Neurophys 1994;71:1797–1825.

Rhode W, Oertel D, Smith P. Physiological response properties of cells labeled intracellularly with horseradish peroxidase in cat ventral cochlear nucleus. J Comp Neurol 1983;213:448–463. [PubMed: 6300200]

Rhode W, Smith P. Encoding of timing and intensity in the ventral cochlear nucleus of the cat. J Neurophysiol 1986;56:261–286. [PubMed: 3760921]

Rose J, Brugge J, Anderson D, Hind J. Phase-locked response to low-frequency tones in single auditory nerve fibers of the squirrel monkey. J Neurophys 1967;30:769–793.

Rothman J, Young E, Manis P. Convergence of auditory nerve fibers onto bushy cells in the ventral cochlear nucleus: Implications of a computational model. J Neurophys 1993;70:2562–2583.

Rothman JS, Young ED. Enhancement of neural synchronization in computational models of ventral cochlear nucleus bushy cells. Aud Neurosci 1996;2:47–62.

Rouiller E, Ryugo D. Intracellular marking of physiologically characterized cells in the ventral cochlear nucleus of the cat. J Comp Neurol 1984;225:167–186. [PubMed: 6327782]

Shofner WP, Sheft S, Guzman SJ. Responses of ventral cochlear nucleus units in the chinchilla to amplitude modulation by low-frequency, two-tone complexes. J Acoust Soc Am 1996;99(6):3592–3605. [PubMed: 8655791]

Smith P, Rhode W. Characterization of HRP-labeled globular bushy cells in the cat anteroventral cochlear nucleus. J Comp Neurol 1987;266:360–375. [PubMed: 3693616]

Smith PH, Rhode WS. Structural and functional properties distinguish two types of multipolar cells in the ventral cochelar nucleus. J Comp Neurol 1989;282:595–616. [PubMed: 2723154]

Stevens, KN. Applying phonetic knowledge to lexical access. Fourth European Conference on Speech Communication and Technology; Madrid, Spain. 1995. p. 3-11.

Tolbert L, Morest D. The neuronal architecture of the anteroventral cochlear nucleus of the cat in the region of the cochlear nerve root: Golgi and nissl methods. Neuroscience 1982;7:3013–3030. [PubMed: 6186942]

Weiss, TF. Electrical Properties. 2. MIT Press; Cambridge, MA: 1995. Cellular Biophysics.

Westerman L, Smith R. A diffusion model of the transient response of the cochlear inner hair cell synapse. J Acoust Soc Am 1988;83:2266–2276. [PubMed: 3411018]

Winter I, Palmer A. Level dependence of cochlear nucleus onset unit responses and facilitation by second tones or broadband noise. J Neurophys 1995;73:141–159.

Wu S, Oertel D. Intracellular injection with horseradish peroxidase of physiologically characterized stellate and bushy cells in slices of mouse anteroventral cochlear nucleus. J Neurosci 1984;4:1577–1588. [PubMed: 6726347]

Young E, Robert JM, Shofner W. Regularity and latency of units in ventral cochlear nucleus: Implications for unit classification and generation of response properties. J Neurophy 1988;60:1–29.

Zurek, PM. The precedence effect. In: Yost, WA.; Gourevitch, G., editors. Direction Hearing. Springer-Verlag; New York: 1987.
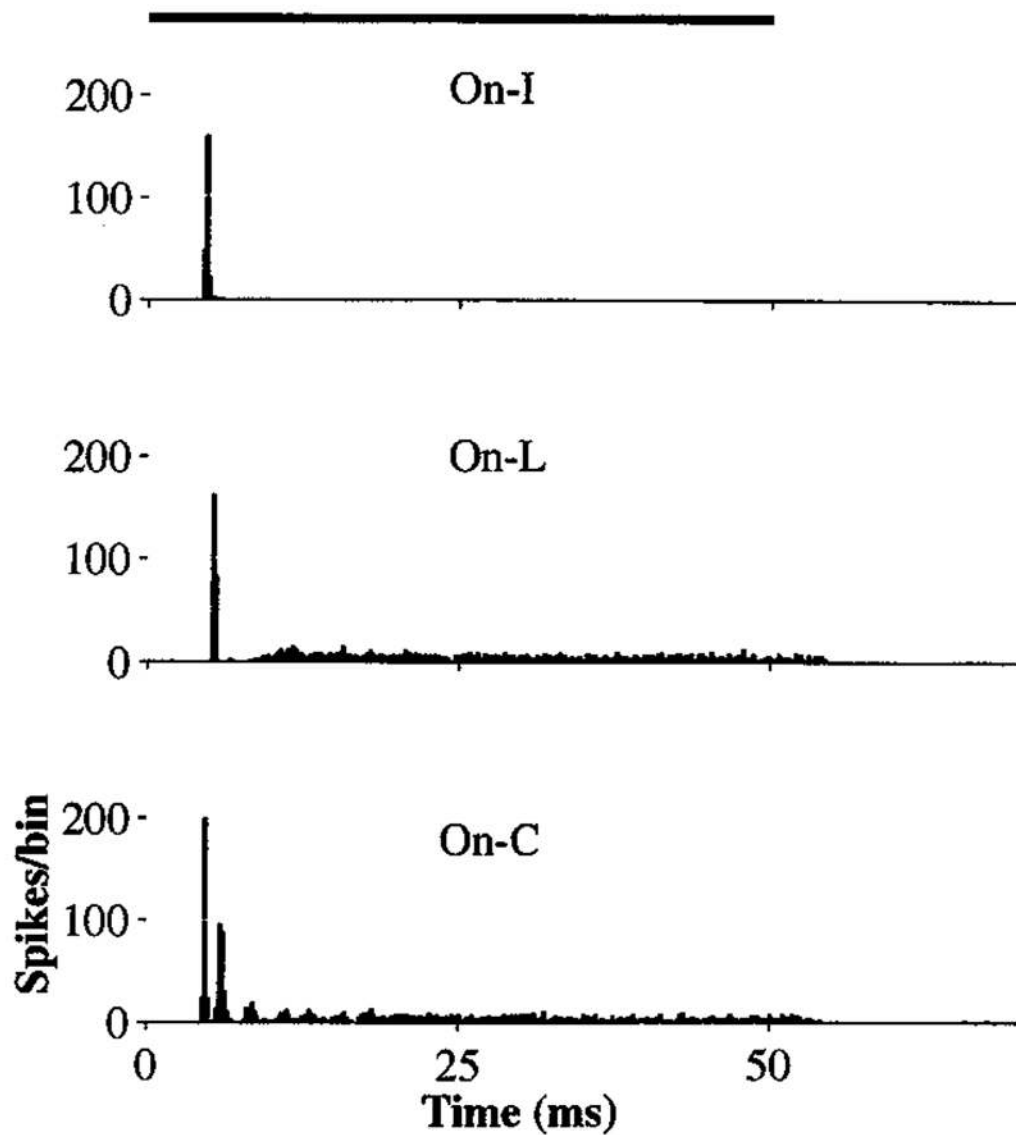
Figure 1.
Peri-stimulus time (PST) histograms for high-frequency tone bursts recorded from *On* neurons in the VCN (from Winter and Palmer, 1995). These are representative examples of the three main classes from the classification scheme of Godfrey et al. (1975a, 1975b) and Rhode and Smith (1986). In each case, the stimulus level is 50 dB above threshold. Bar above the top PST histogram indicates the duration of the stimulus. There were 250 stimulus presentations and the binwidth was 0.2 milliseconds.
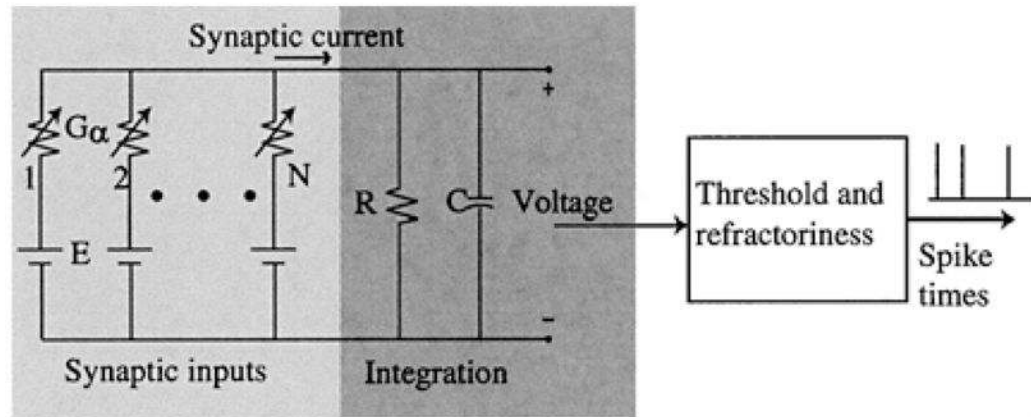
Figure 2.
An integrate-to-threshold point-neuron model.
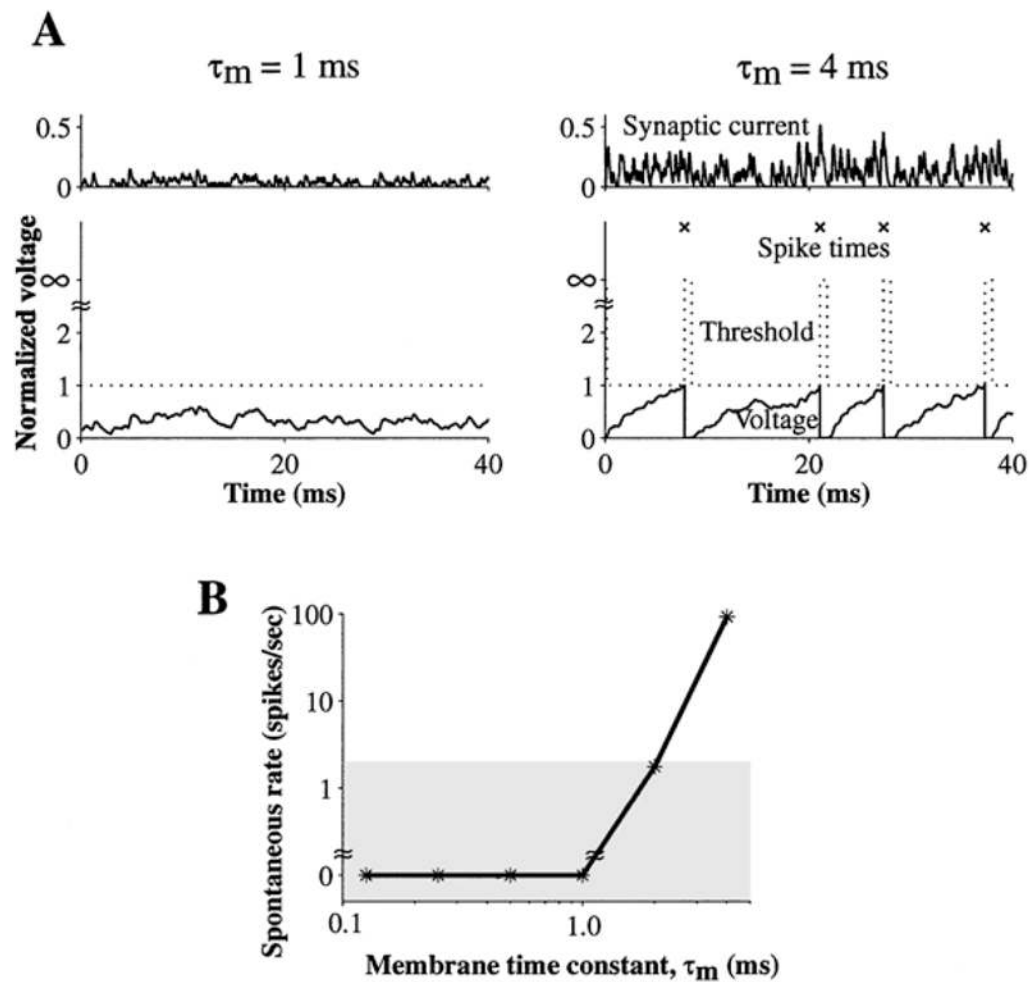
Figure 3.
Spontaneous discharge rate in the leaky-integrator model. The number of inputs, N, is 100 and the synaptic strength, G_α, is 1/20. (**A**) Example traces of synaptic current, membrane voltage, threshold, and spike times of the leaky-integrator model during spontaneous activity. These variables correspond to quantities labeled in Fig. 2. There is an absolute refractory period during which there can be no spike discharges and immediately after which the membrane voltage and the threshold are reset to their resting values. The membrane time constant, τ_m, is equal to 1 ms and 4 ms in the left and right panel respectively. The synaptic current is different despite the same N and G_α in the two panels because the synaptic conductance is normalized by a greater unitary synaptic strength (see Methods) when $\tau_m = 1$ ms. (**B**) Spontaneous rate as a function of τ_m. The grey-shaded region indicates the range for *On* neurons in the data.
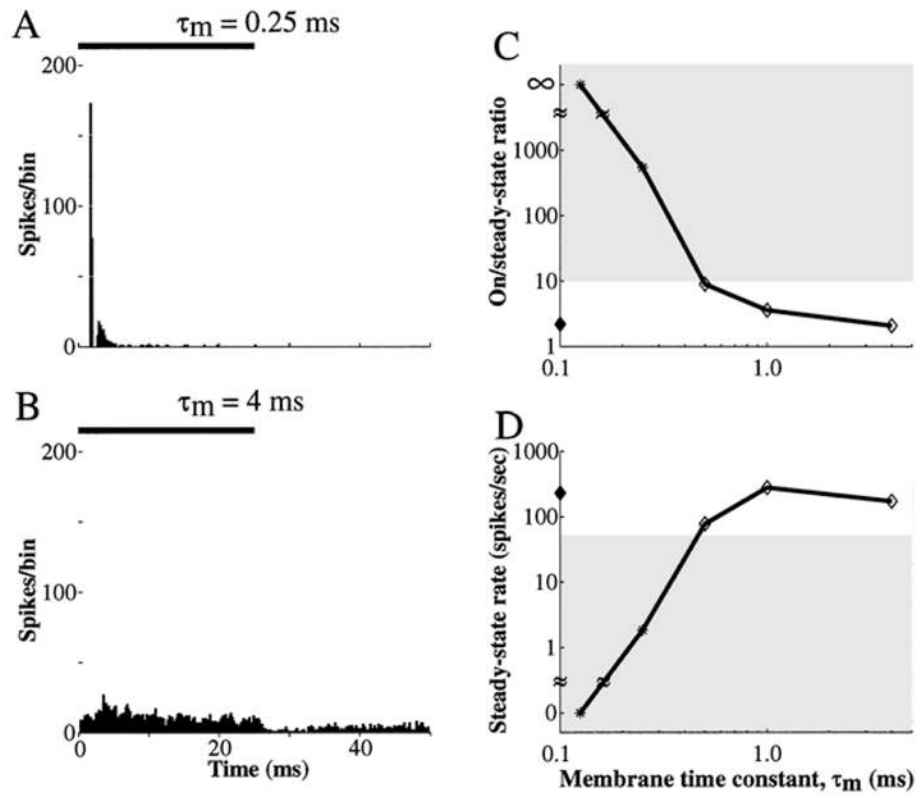
Figure 4.

Peri-stimulus time (PST) histograms for characteristic frequency (CF) tone bursts as a function of τ_m. (**A** and **B**) PST histograms for CF (6000 Hz) tone bursts, 20 dB above threshold, with $\tau_m = 0.25$ ms and $\tau_m = 4$ ms respectively (250 stimuli, binwidth = 0.2 ms). Bars above the histograms indicate duration of the stimulus. (**C**) Ratio of onset rate to steady-state rate and (**D**) steady-state discharge rate measured from PST histograms, as in A and B. Corresponding measures from the response of a model AN fiber to a CF (6000 Hz) tone burst are indicated by filled ◇s on the ordinate. Grey shading shows the range of the measures for *On* neurons in the data. A ✶ plot symbol indicates that the shape of the PST histogram satisfies both criteria (On/steady-state ratio and steady-state rate) for an *On* PST histogram while an unfilled ◇ plot symbol indicates that the PST histogram fails to satisfy either one or both of the criteria. Further details on these criteria are in Methods. For all panels, $N = 100$ and $G_\alpha = 1/20$.
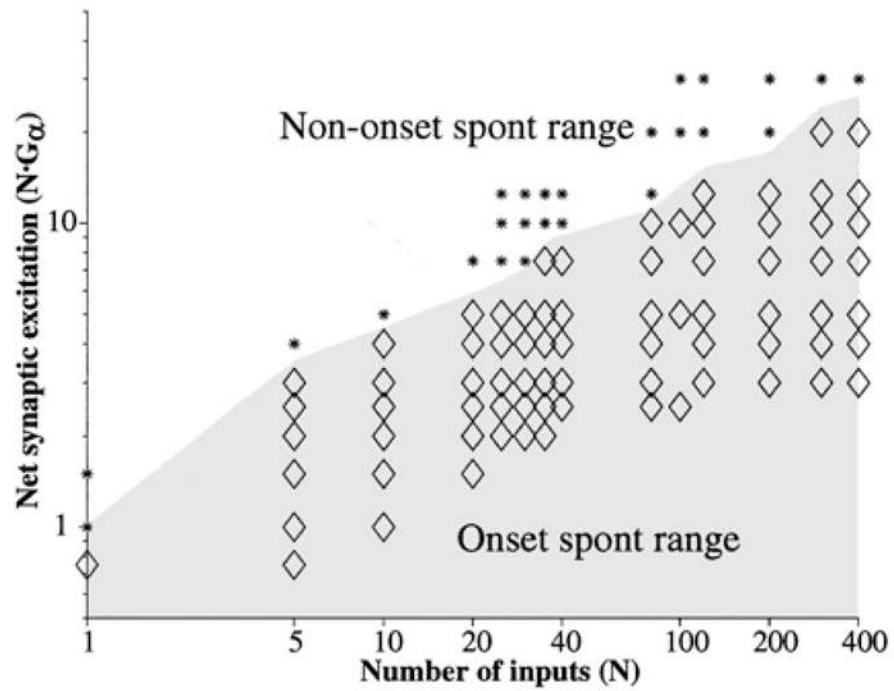
Figure 5.
Spontaneous rate as a function of N and the net synaptic strength, $N \cdot G_\alpha$, in the leaky-integrator model. The plot symbols indicate different types of spontaneous discharge ($\diamond$ and grey shading: spontaneous rate in the *On* range, $\star$: spontaneous rate too high). $\tau_m = 0.125$ ms in this figure and for the remaining figures in the paper.
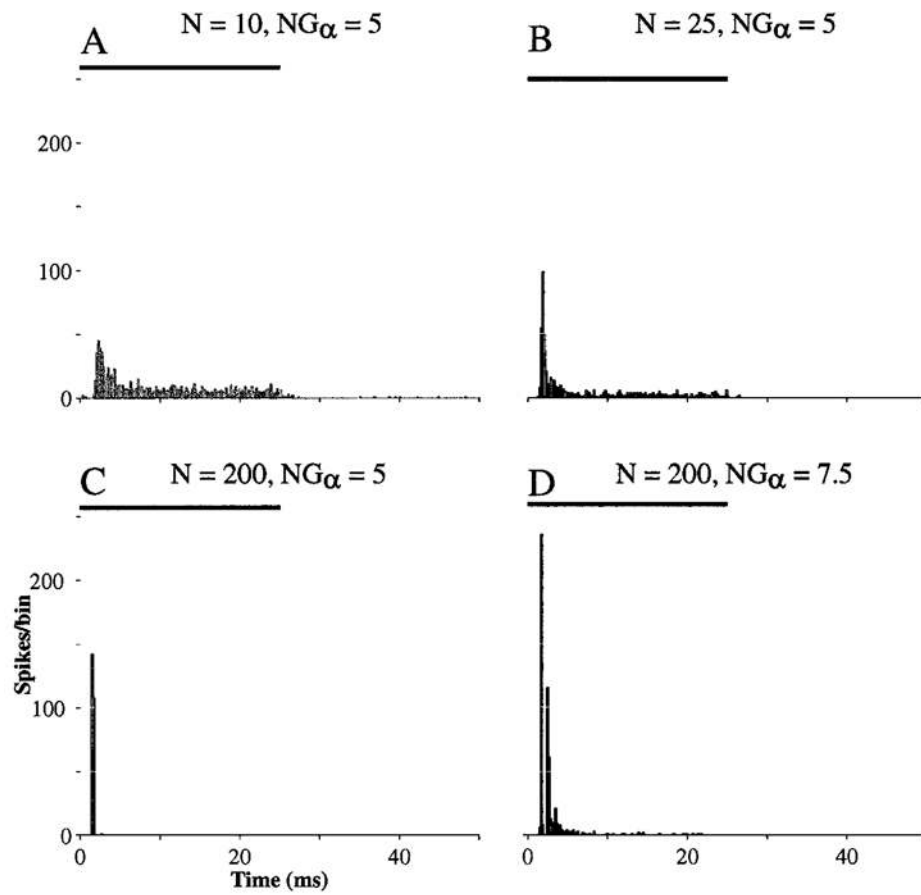
Figure 6.
PST histograms for 6000 Hz tone bursts as a function of N and G_α in the leaky-integrator model. The stimuli are presented at 20 dB above threshold. Bars above histograms indicate the duration of the stimulus.
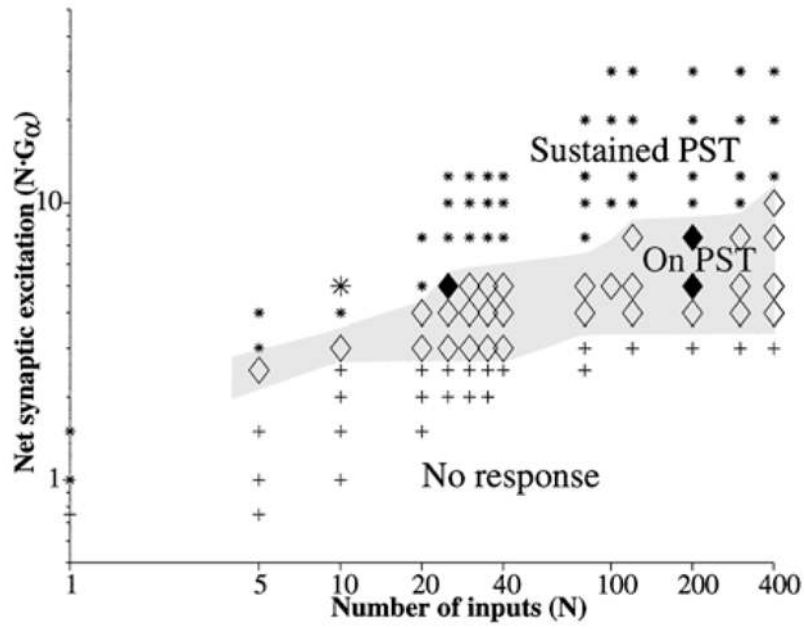
Figure 7.
The type of PST histogram for CF tone bursts for pairs of N and $N \cdot G_\alpha$. The plot symbols indicate different types of PST histograms ($\diamondsuit$ and grey shading: *On* PST type, $\star$: *Sustained* PST type, +: no response). The PST type is "no response" when the threshold is greater than 70 dB SPL. The big $\star$ and the filled $\diamondsuit$s identify the four pairs of N and $N \cdot G_\alpha$ in Fig. 6
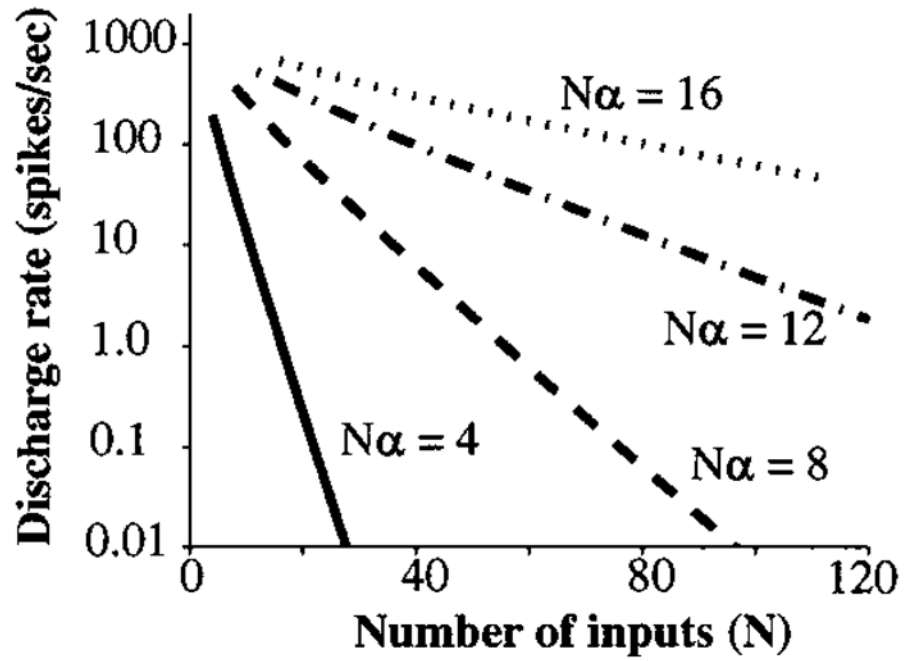
Figure 8.
Spontaneous rate of an analytical coincidence-detector model as a function of the number of inputs. Each curve corresponds to a fixed net synaptic strength, $N \cdot \alpha$. The duration of the coincidence window, $\varDelta t$, is 0.5 ms.
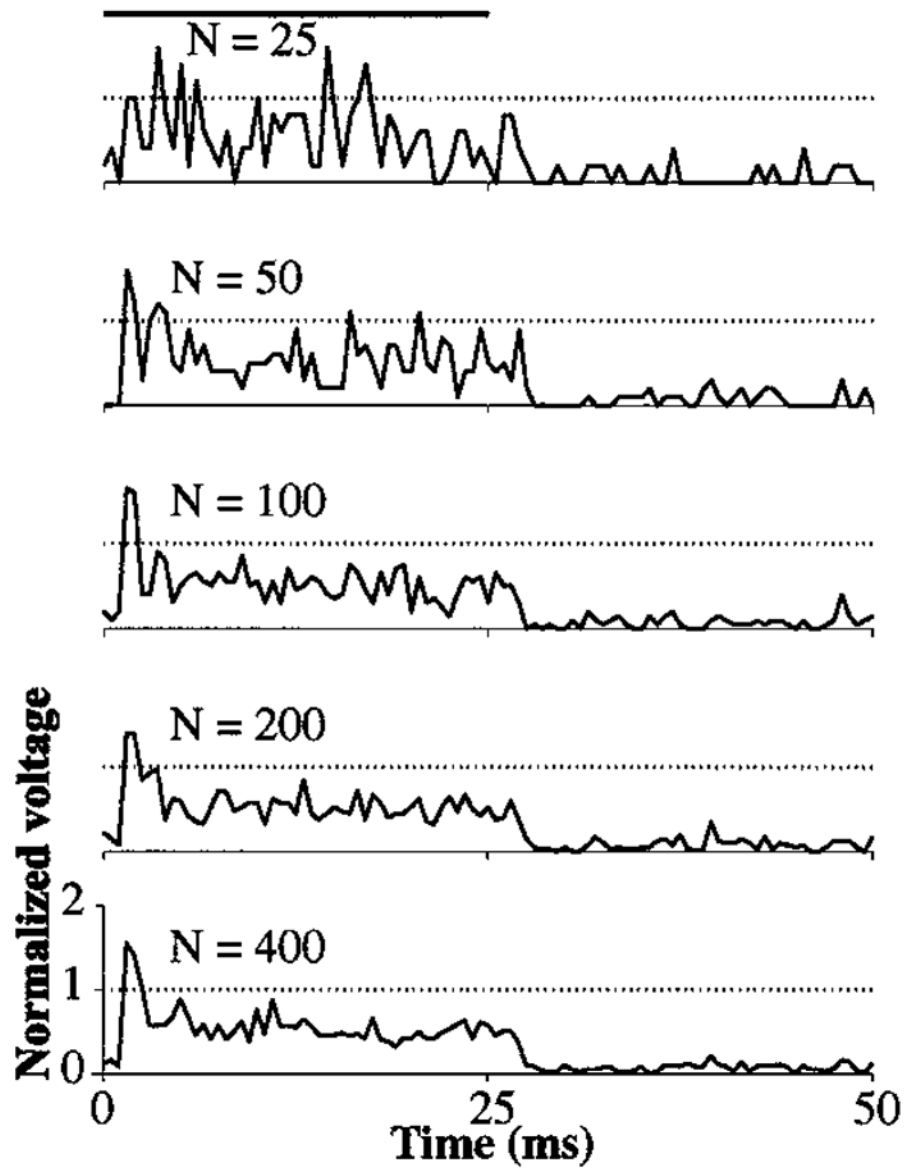
Figure 9.
Typical traces of intracellular voltage in the analytical model due to a 6000 Hz, 60 dB SPL tone burst for different values of N. The dotted line is the threshold for spiking. Bar indicates duration of the stimulus. $N \cdot \alpha = 5$ and $\Delta t = 0.5$ ms.
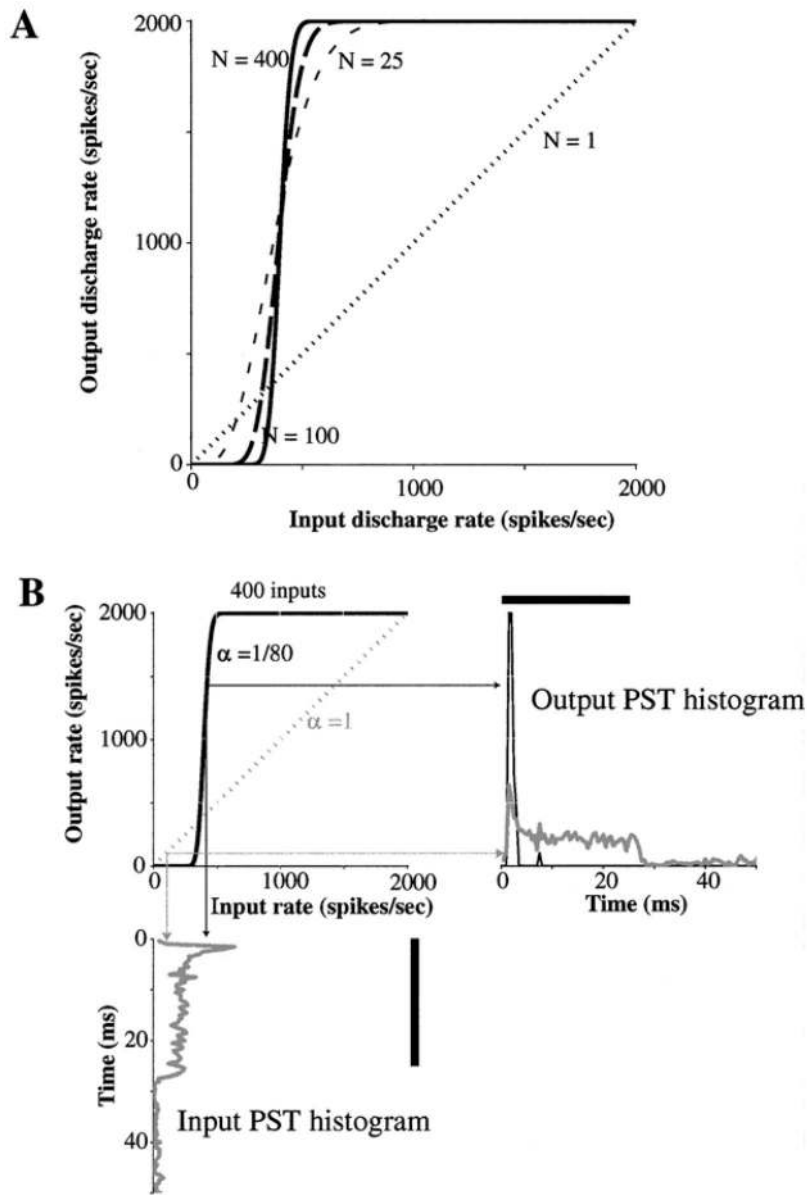
Figure 10.
The transformation of input to output in the analytical coincidence detector model. (**A**) The instantaneous relationshp between output discharge rate and discharge rate of the inputs for different values of *N*. (**B**) Transformation of the *Sustained* PST histogram of the inputs (model AN response to 60 dB SPL, 6000 Hz tone burst) to an *On* PST histogram for $N = 1$ and $N = 400$. $N \cdot \alpha = 5$ and $\Delta t = 0.5$ ms for all curves.
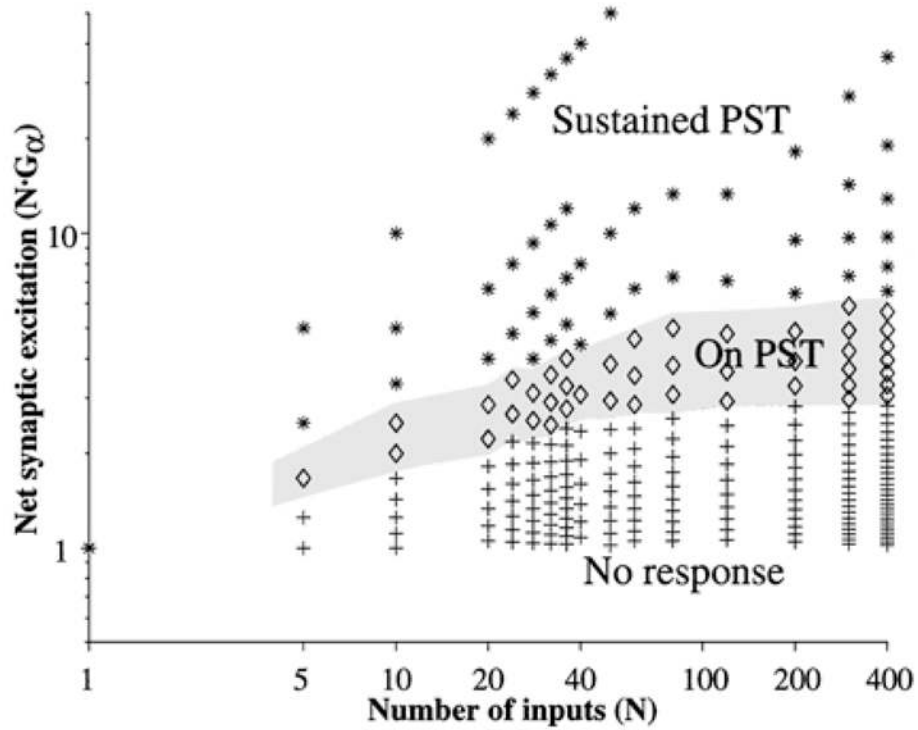
Figure 11.
The shape of PST histograms for high-frequency tone-bursts (6000 Hz, 60 dB SPL) as a function of N and $N \cdot \alpha$ in the analytical coincidence-detector model. The format of this figure is the same as the format of Fig. 7. The criteria for classifying the type of response are the same as in Fig. 4 except that the "no response" classification is used if the discharge rate for the tone burst is less than 10 spikes/sec. This 10 spikes/sec discharge rate is the criterion rate used for determining the threshold CF-tone burst level in the leaky-integrator model. $\Delta t = 0.5$ ms.
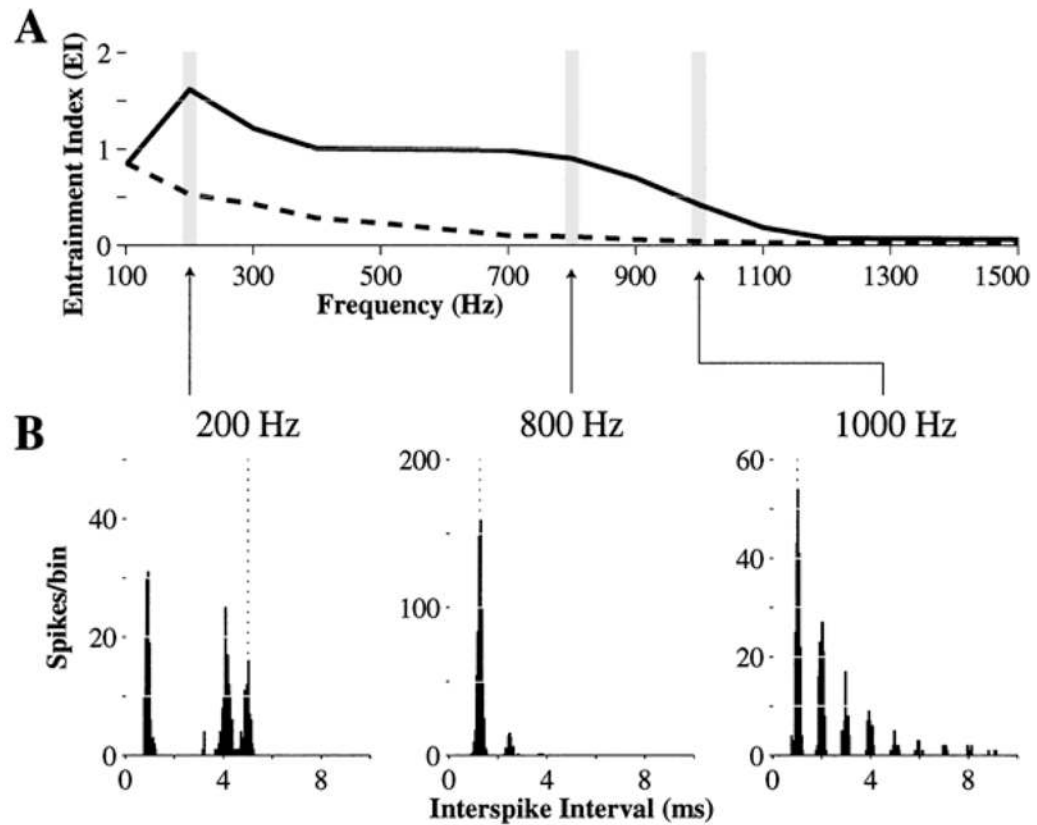
Figure 12.
Entrainment to low-frequency tones in the leaky-integrator model. (**A**) Entrainment index (*EI*) as a function of tone frequency for the leaky-integrator model (solid) and for a model AN fiber with a CF of 6000 Hz (dashed). (**B**) Histograms of intervals between consecutive spikes for a 200 Hz tone, an 800 Hz tone, and a 1000 Hz tone (all at 90 dB SPL). The vertical dotted lines in the three graphs are at the stimulus periods. $N = 400$ and $N \cdot G_\alpha = 8.8$.
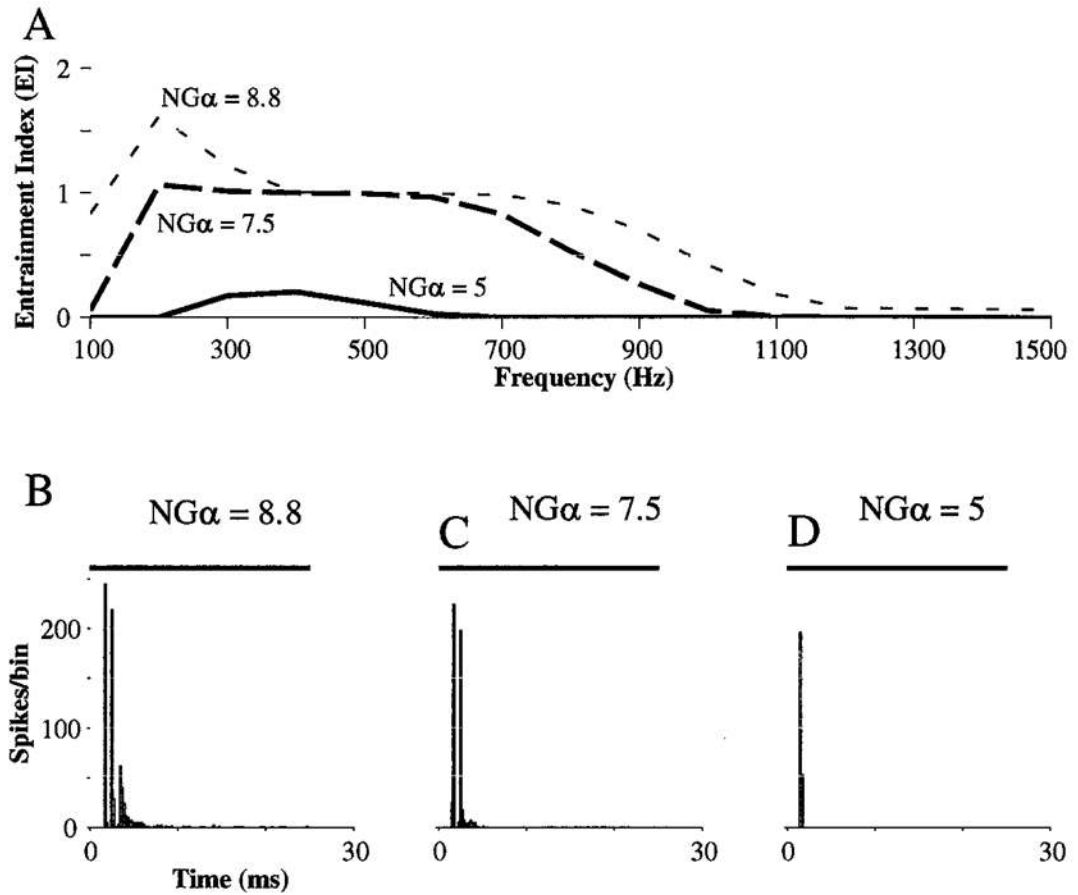
Figure 13.
Entrainment to low-frequency tones and PST histograms for 6000 Hz tone bursts as a function of $N \cdot G_\alpha$ in the leaky integrator model. (**A**) *EI* as a function of frequency for $N \cdot G_\alpha$ equal to 8.8, 7.5, and 5, with *N* held constant at 400. (**B, C** and **D**) PST histograms for 6000 Hz tone bursts at 20 above threshold, with $N = 400$.

Table 1

Summary of parameters of the leaky-integrator model.

Variable	Description	Range or value
N	Number of inputs	1–2000
$N \cdot G_\alpha$	Net synaptic strength	1–30
τ_m	Membrane time constant	0.125–4 ms
T_r	Refractory period	0.7 ms
τ_s	Synaptic time constant	0.1 ms
E/θ_0	Synaptic reversal potential (normalized)	8.57
$4 \cdot \sigma_{CF}$	CF range of AN inputs	1 octave